Biological and Medical Applications of Materials and Interfaces

3D DNA origami as programmable anchoring points for bioreceptors in fiber optic surface plasmon resonance biosensing

Devin Daems, Wolfgang Pfeifer, Iene Rutten, Barbara Sacca, Dragana Spasic, and Jeroen Lammertyn

ACS Appl. Mater. Interfaces, **Just Accepted Manuscript** • DOI: 10.1021/acsami.8b04757 • Publication Date (Web): 27 Jun 2018

3D DNA origami as programmable anchoring points for bioreceptors in fiber optic surface plasmon resonance biosensing

Devin Daems[1], Wolfgang Pfeifer[2], Iene Rutten[1], Barbara Saccà[2], Dragana Spasic[1,*], Jeroen Lammertyn[1,*]

[1]KU Leuven - University of Leuven, Department of Biosystems, MeBioS-Biosensors group, Willem de Croylaan 42, B-3001 Leuven, Belgium

[2]University of Duisburg-Essen, Centre for Medical Biotechnology (ZMB), Universitätstrasse 2, 45117, Essen, Germany

[*] Corresponding authors: jeroen.lammertyn@kuleuven.be; dragana.spasic@kuleuven.be, +32 16 321459.

Abstract

Many challenges in biosensing originate from the fact that the all-important nano-architecture of the biosensor's surface, including precise density and orientation of bioreceptors, is not entirely comprehended. Here we introduced a 3D DNA origami as bioreceptor carrier to functionalize the fiber optic surface plasmon resonance (FO–SPR) sensor with nanoscale precision. Starting from a 24-helix bundle, two distinct DNA origami structures were designed to position thrombin-specific aptamers with different density and distance (27 and 113 nm) from the FO-SPR surface. The origami-based biosensors proved to be not only capable of reproducible, label-free thrombin detection, but revealed also valuable innovative features: (1) a significantly better performance in the absence of backfilling, known as essential in biosensing field, suggesting improved bioreceptor orientation and accessibility and (2) a wider linear range compared to previously reported thrombin biosensors. We envisage that our method will be beneficial both for scientists and clinicians looking for new surface (bio)chemistry and improved diagnostics.

Keywords: DNA origami, aptamer, biosensor, fiber optic SPR, nanostructuring

1. Introduction

Although the first biosensor[1] has been developed already 50 years ago[2,3] and tremendous progress has been made since then, designing an ASSURED (Affordable, Sensitive, Specific, User-friendly, Rapid and Robust, Equipment-free and Deliverable to end users) biosensor is still a challenge[4]. One of the major difficulties is to establish highly specific and sensitive biomolecular detection concepts while keeping the complexity and thus the cost of the biosensor at an acceptable level.

For many years scientists have been acknowledging the importance of the affinity of bioreceptors in the process of biomolecular detection. However, the nano-architecture of the biosensing surface (i.e. the precise density, orientation and arrangement of coupled bioreceptors) is often neglected or not fully understood. Consequently, the majority of the biosensors are still constructed on the basis of a classic two-step assembly strategy: first, a bulky coupling of the bioreceptors to the sensor surface through different immobilization concepts (covalent attachment, affinity immobilization, self-assembly, etc.), followed by backfilling of the unoccupied areas to limit unspecific binding of other molecules present in the sample. Despite being robust, many of the available surface chemistries remain largely empirical and mostly uncontrolled. Therefore, to engineer controlled, stable and well-defined biosensing interfaces with nanoscale precision it is critically important to improve our understanding and manipulation of bioreceptor coupling and surface (bio)chemistry[5,6].

Notable progress in this research area has been achieved by combining bioreceptors with DNA nanostructures of programmable shape and pattern, ranging from the first reported immobile structure (i.e. Holliday junction[7]) up to the large (e.g. 100 µm) two-dimensional (2D) DNA lattices[8] and three-dimensional (3D) cube[9] or a tetrahedron[10-11]. Thus, by implementing DNA tetrahedrons on electrochemical biosensors as anchoring points for bioreceptor molecules, significant improvement has been accomplished in controlling the density, orientation, stability and distance of the receptor molecules on the surface.[12] Based on this knowledge, a variety of other electrochemical and optical biosensors have been constructed using 2D and 3D DNA nanostructures for the detection of DNA targets (hybridization, single nucleotide polymorphisms and genotyping), proteins and small molecules, resulting in biosensors with a higher accessibility of the bioreceptors[12-14].

Despite this major progress, several issues still remain unsolved when using DNA tetrahedrons: (i) the instability of the DNA tetrahedrons upon small changes in pH, salt concentration and temperature, (ii) the limited surface addressability of the DNA tetrahedron design that prevents implementing precisely controlled distributions of multiple bioreceptors, (iii) the high flexibility of the DNA tetrahedrons, which affects reorganization of the number/orientation of the bioreceptors per DNA tetrahedron and (iv) the need for backfilling molecules to prevent nonspecific adsorption of targets to the biosensor surface.

The introduction of the scaffolded DNA origami in 2006[15] enormously contributed to the development of structural DNA nanotechnology, allowing to engineer various 2D and 3D structures of increasing complexity and mechanical robustness[16-19]. The DNA origami method relies on the nanoscale folding of a long, single stranded (ss) DNA (known as “scaffold”) into a 2D or 3D shape through hybridisation to hundreds of oligonucleotides (known as “staple strands”) used to hold the scaffold in place. Different applications have been reported so far for DNA origami structures in material science[20-23], biomolecular interaction analysis[24-26], molecular computation[27] and nanomedicine[28-31]. Recently, it has been shown that the thermostable and rigid DNA origami technique [32] was used to incorporate multiple bioreceptors, which preserve their ability to specifically bind their target of interest [26, 33]. Moreover, it was demonstrated that DNA origami can be used in biosensing as nanoantennas[34, 35] or nanorobots[36].

The aim of this work is to exploit 3D DNA origami for the first time to nano-pattern a biosensing surface of a surface plasmon resonance (SPR) device. For this purpose, we engineered rigid DNA origami

structures modified at their distal ends (DE) or lateral surfaces (LS) with two distinct sets of ssDNA: one set for specific attachment of DNA origami structures to the biosensor surface (will be referred to as ssDNA set 1) and the other set for specific attachment of bioreceptors to the DNA origami (will be referred to as ssDNA set 2). Furthermore, we studied the developed DNA origami structures with respect to stability, orientation, accessibility and spatial density of the attached bioreceptors. We also investigated the suitability of the DNA origami structures for the functionalization of the biosensor surface, being an in-house developed Fiber Optic Surface Plasmon Resonance (FO-SPR) sensor platform[37-43], by looking into the density and relative orientation of the bioreceptors as well as their distance from the sensor surface. Finally, we applied our method to detect a non-DNA target molecule and compared the need for backfilling in DNA origami and tetrahedron-functionalized FO-SPR biosensors. Our results provide evidence of increased biosensor performance when moving from random to highly-ordered functionalization of the biosensor surface through DNA origami structures.

2. Experimental Section

2.1. Reagents

All chemicals were of analytical reagent grade and purchased from The Merck group – Sigma Aldrich (Diegem, Belgium), unless stated otherwise. Solutions were prepared with deionized water purified by a Milli-Q Plus system (The Merck group - Millipore, Marlborough, MA, USA). Buffers used were:

- 1× TE: 5 mM Tris base, 1 mM Na_2EDTA, pH 8.0
- TM buffer: 20 mM Tris base, 50 mM $MgCl_2$, pH 8.0
- 1× TEMg: 5 mM Tris base, 1 mM Na_2EDTA, 13 mM $MgCl_2$, pH 7.6
- TEMg(16): 5 mM Tris base, 1 mM Na_2EDTA, 16 mM $MgCl_2$, pH 8.0
- TBE: 40 mM Tris base, 20 mM boric acid 2 mM Na_2EDTA, pH 8.0
- 1× TBEMg: 40 mM Tris base, 20 mM boric acid 2 mM Na_2EDTA, 13 mM MgAcetate, pH 8.0
- TNM: 10 mM Tris base, 25 mM $MgCl_2$, 2 M NaCl, pH 8.0
- TGK: 25 mM Tris base, 192 mM Glycine, 5mM K_2HPO_4, 0.1 % Tween20 and 0.15 % w/v BSA, pH 8.3
- PB: 12 mM $K_2HPO_4$and 167 mM K_2HPO_4, pH 8.3
- PB-SDS: 0.676 mM K_2HPO_4, 9.3 mM K_2HPO_4, 0.01 % SDS, pH 8.0
- PEG 8000: 5 mM Tris base, 1 mM Na_2EDTA, 505 mM NaCl, 15 % w/v PEG 8000 (Roth, Karlsruhe, Germany)

All unmodified, biotin-modified and thiol-modified oligonucleotides were purchased from Integrated DNA technologies (IDT, Haasrode, Belgium) as desalted products and delivered lyophilized in 96-well plates or vials (Supporting Information Table S1, S2, S3 and S4). Amicon Ultra 0.5 mL centrifugal Filter devices were purchased from Millipore. Freeze 'N Squeeze DNA Gel Extraction Spin Columns were obtained from BIO-RAD (USA). NAP-5 columns were obtained from GE Healthcare (Diegem, Belgium). Human-α-Thrombin was purchased from Bio-Connect (Huissen, The Netherlands) while streptavidin and tris (2-carboxyethyl) phosphine hydrochloride (TCEP) were obtained from ThermoFisher Scientific (Geel, Belgium). Ligand free Au NPs obtained by laser ablation, with a mean diameter of 25 ± 6 nm, were kindly provided by Prof. S. Barcikowksi (University of Duisburg-Essen, Germany). 1,4-dithiotreitol (DTT) was purchased from VWR International (Geel, Belgium). The 1 kb and 100 bp DNA ladders were purchased from Roth (Karlsruhe, Germany) and Invitrogen (Merelbeke, Belgium), respectively.

2.2. Design and assembly of the 3D DNA origami structures

Two 3D DNA origami structures (LS and DE) were designed using caDNAno (caDNAno 2.2.0, MIT License, USA)[44] and visualized with Maya 2015 (Autodesk.Inc, California, USA). The complete list of oligonucleotide sequences used for folding the M13mp18 single-stranded DNA scaffold into the desired shapes is shown in Supporting Information Figures S1 and S2 and Tables S3 and S4. These two DNA origami structures were based on a similar 24 helix bundle previously reported in literature[45] and have been designed in a way that one side can couple to a gold surface and the opposite side can hybridize to a bioreceptor. This is important for functionalizing origami structures on the sensor surface in different directions.

Three different ways of assembling the LS and DE origami structures with attached bioreceptors and thiol-modified ssDNA strands on predefined positions were explored: (i) 1-step assembly of the bundle with ssDNA set 1 and 2, bioreceptor and thiol-modified oligonucleotides, (ii) 2-step assembly hybridizing the bioreceptor and thiol-modified oligonucleotides to a pre-assembled bundle with ssDNA set 1 and 2 for 1 h (at 37 °C), or (III) similar 2-step assembly with intermediate PEG purification. One-step assembly of DNA origami structures was done according to Rothemund's procedure[15], using a 1:20 molar ratio between the single-stranded DNA scaffold and each of the staple strands in 1× TEMg buffer in a total volume of 1 mL, unless stated otherwise. The annealing was performed by decreasing the temperature from 65 °C to 55 °C (ramp speed: -1 °C/5 min), 55 °C to 30 °C (ramp speed: -1 °C/15 min) and 30 °C to 20 °C (ramp speed: -1 °C/min) using a Thermocycler Nexus Gradient (Eppendorf, Rotselaar, Belgium).

2.3. Gel electrophoresis

Unless stated otherwise, 3D DNA origami structures were run on a 1 % agarose gel using a loading dye (50 % glycerol, 10 % 10x TE buffer, 40 % H_2O and traces of bromophenolblue) with 1× TBEMg for 2.5 h (at 80 V) and stained with ethidium bromide (15 min). Band intensities were visualized with Typhoon FLA 9000 (GE Healthcare Life Sciences, Diegem, Belgium).

2.4. Purification of DNA origami structures

The FNS purification method started with a careful excision of the band of interest, containing the DNA origami structures, from the 1 % agarose gel stained with ethidium bromide. Afterwards, the gel slice was placed into the FNS gel extraction spin column and stored at -20 °C for 5 min. After centrifugation of the sample for 3 min at 13000 g (room temperature), the purified DNA origami nanostructures were collected from the collection tube.

The PP method was based on Stahl et al[46]. In short, self-assembly reaction mixtures, containing DNA origami and the excess of staple strands together with bioreceptors and/or thiol-modified ssDNA strands, were mixed in 1:1 (v/v) ratio with PEG 8000 precipitation buffer. The samples, originally containing 13 mM $MgCl_2$, were adjusted to reach a final $MgCl_2$ concentration of 10 mM using 100 mM $MgCl_2$. The solutions were mixed by inversion and centrifuged at 16000 g, at room temperature for 25 min using a microcentrifuge (VRW, Leuven, Belgium). Afterwards, the supernatant was removed. Finally, the pellet was dissolved in TEMg buffer, unless stated otherwise, for approximately 30 min at 30 °C.

The SCP method started with washing the Amicon Ultra 0.5 mL centrifugal filter devices with 500 µL of TEMg (containing 6 mM $MgCl_2$) by centrifugation at 10000 g for 5 min. Afterwards, 50 µL of a DNA origami sample was added to the device together with 450 µL of TEMg and centrifuged for 5 min at 4500

g. After removing the excess of staple strands, approximately 15 µL of DNA origami nanostructures were recovered by reverse spinning of the centrifugal filter device.

2.5. AFM

For AFM imaging, typically 5 µL of sample was applied onto freshly cleaved mica (Plano GmbH, Wetzlar, Germany) and left to adsorb for 3 min at room temperature. 2.5 µL of self-assembled (and purified) DNA origami structures was diluted by adding it to 2.5 µL of TEMg(16) buffer on the mica. Afterwards, the sample was washed with ddH_2O and dried under a gentle stream of argon. Imaging was performed on a MultiMode VIII (Bruker, Karlsruhe, Germany) in air, using ScanAsyst-Air probes (nominal radius of 2nm and max radius of 12 nm) with 0.4 N/m force constant cantilevers (Bruker, Karlsruhe, Germany). Images were analyzed by using Brukers software Nanoscope analysis (v8.15).

2.6. Formation of DNA tetrahedron structures

Four oligonucleotides (tetra-B (B), tetra-C (C), tetra-D (D) and tetra-A (A) or tetra-T (T), Supporting Information Table S2)[47] were mixed together in equimolar quantities in TM buffer, heated for 2 min to 95 °C and then cooled to 4 °C (ramp speed -0.5°C/min) (Supporting Information Figure S3). The tetrahedron mixture consisted of 4 µL of each oligonucleotide solution (1 µM of B, C, D and T) mixed with 164 µL TM buffer and 20 µL TCEP (3 mM), unless stated otherwise. The DNA tetrahedrons (15 µL with 10 µL loading buffer (Novex Hi-density TBA sample buffer, Thermo Fisher Scientific, Geel, Belgium)) were analyzed using a 10 % Novex TBE Gel (Invitrogen, Merelbeke, Belgium) in TBE running buffer at 500 mA for 105 min in a XCell SureLock Mini-Cell Electrophoresis System (Invitrogen) connected to a 250-90 Electrophoresis Power Supply (Thermo Electron Corporation, Milford, MA, USA) and stained with SYBR green (ThermoFisher Scientific, Geel, Belgium) for 30 min.

2.7. FO-SPR

The FO-SPR device and manufacturing of the FO-SPR sensors were previously described by Knez et al.[41, 42] The fabricated, bare FO-SPR sensors have a very high reproducibility (CV ≤ 4%). Thiol-modified ssDNA (i.e. hybridization probes for binding the DNA origami structures) were immobilized on the FO-SPR sensor tips by adding 1 µM of DNA, previously activated with 0.1 M DTT in PB buffer. DTT was used to break up thiol dimers that could inhibit the surface functionalization and was removed from the solution by DNA purification with a NAP-5 column (GE Healthcare, Oslo, Norway). FO-SPR sensor surfaces were then washed three times in PB with 0.01 % SDS and stored in the same buffer at 4 °C until further use. In a second step, DNA origami structures consisting of a bundle, ssDNA set 1, ssDNA set 2 and bioreceptors, and purified following the PP method, were added with a concentration of 16 nM (LS, occupied surface 1573 nm²/origami) or 83 nM (DE, occupied surface 227 nm²/origami) to the FO-SPR sensor tip surfaces in TNM buffer and left overnight at 4 °C to hybridize to the thiol-modified ssDNA attached to the sensor tip surface. Theoretically, 4.8×10^9 LS structures and 3.3×10^{10} DE structures can attach to the FO-SPR biosensor surface (7.5×10^{12} nm²). Finally, functionalized FO-SPR sensor tips were washed with TGK and stored at 4 °C in the same buffer until further use.

For immobilizing tetrahedron structures (occupied surface 15 nm²/tetrahedron), FO-SPR sensor tips were incubated overnight at 4 °C in 200 µL of tetrahedron mixture (40 nM), containing TCEP to activate the thiol groups. Theoretically, 4.9×10^{11} DNA tetrahedrons can attach to the FO-SPR biosensor surface. Backfilling of the FO-SPR sensor tips was done directly prior the use in the bioassay, by incubating in 50 µM alkane thiol PEG (PEG MUA, Polypure, Oslo, Norway) in TEMg (DNA origami) or TM (tetrahedron) for

1 h. Afterwards, functionalized FO-SPR sensor tips were washed three times with a 0.01 % SDS PB and stored at 4 °C in H_2O, or TGK buffer in the case of tetrahedrons, until further use.

To check the accessibility of the TBA bioreceptors immobilized on the FO-SPR sensor tips through DNA nanostructures, the sensor tip was immersed for 25 min in a solution containing 100 nM atto-labeled oligonucleotides (complementary to the TBA aptamer, Supporting Information Table S1) at 37 °C, followed by a short washing step of 3 min in TGK buffer at 37 °C. Prepared FO-SPR sensors were immediately taken for the imaging with fluorescent microscope as explained in the next section.

For performing the thrombin bioassay, the FO-SPR sensor tip was immersed in 120 µL TGK buffer (5 min) to reach a stable baseline. Next, the FO-SPR sensor tip (single measurement per FO-SPR sensor) was immersed in the thrombin solution with a concentration of 0, 15.5, 31, 62, 124 or 248 nM in TGK buffer for 20 min, followed by a short washing step of 3 min in TGK buffer.

FO-SPR data were recorded with LabView (National Instruments, Austin, TX, USA) and further processed using Origin 8 (OriginLab, USA). Calibration curves were fitted with a one-site binding fit[38]:

$$y = \frac{x \times A}{x + B} \quad (1)$$

where *y* is the SPR shift (nm), *x* represents the thrombin concentration (nM), whereas the fitting parameters *A* and *B* represent the maximum specific binding (nm) and the equilibrium binding constant (nM), respectively.

Equation 2 was used to calculate the LOD of the established bioassays:

$$LOD = y_0 + 3 \times s_0 \quad (2)$$

with y_0 being the average response for 0 nM thrombin and s_0 the mean standard deviation for y_0.

2.8. Fluorescent microscopy

The presence of fluorescent oligonucleotides coupled to DNA structures on the FO-SPR sensor tip surface was determined using an inverted fluorescence microscope (IX71, Olympus Corporation, Japan) with a mercury lamp, 20× objective and EM-CCD camera (Hamamatsu Photonics K.K., Japan). To select the correct excitation and emission wavelength, a WIBA filter (excitation filter BP530-550, emission filter BA575-625, and dichromatic filter DM570) was used for imaging.

3. Results and Discussion

3.1. 3D DNA origami development and characterization

In this paper, we developed two DNA origami structures, based on a previously reported 24-helix bundle[45]. For both structures, the 24-helix bundle was modified using two different sets of ssDNA strands (Figure 1A and B). ssDNA set 1 (represented in light red in all the figures) was designed to allow specific attachment of DNA origami structures to the biosensor surface through hybridization to complementary thiol-modified ssDNA immobilized on the sensor (dark red representation in all the figures). ssDNA set 2 (represented in light green in all the figures) was designed to enable specific hybridization of bioreceptors (dark green representation in all the figures) to the DNA origami. Here, two different bioreceptors were used: (i) biotinylated ssDNA (for specific binding to streptavidin) or (ii)

thrombin binding aptamer (TBA) specifically recognizing the heparin binding domain (exosite II) of the human α-thrombin[48].

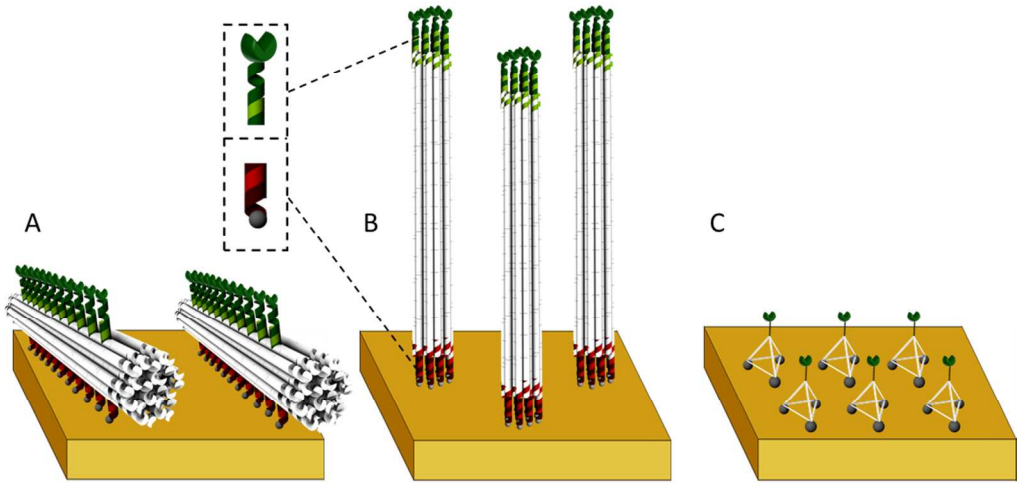

Figure 1: Schematic overview of bioreceptor patterning onto a gold surface using DNA nanotechnology (not to scale): 3D DNA LS origami (A), 3D DNA DE origami (B) and 3D DNA tetrahedron (C), containing bioreceptors (dark green) and thiol groups (dark grey spheres) for surface attachment. Zoom-in: representation of the distinct set of ssDNA (light green) for specific attachment of the bioreceptors (dark green) to the DNA origami and the distinct set of ssDNA (light red) for specific attachment of the DNA origami structures to the biosensing surface (dark red).

However, to achieve different orientations of the DNA origami structures on the sensor surface, ssDNA set 1 and 2 were positioned along the lateral surface of the bundle (referred to as LS) and at the the distal ends of the bundle (referred to as DE), respectively. (Figure 1A and B). Importantly, in each structure, the two sets of ssDNA were positioned opposite one another leading to a bundle with 11 elongated staples at the lateral sides or 12 elongated staples at the distal ends (Figure 2A-B, for the LS and DE configuration, respectively).

In order to make robust DNA origami structures[49] for reproducible biosensing experiments, we first evaluated their stability under different buffer conditions. More specifically we analysed the effect of different $MgCl_2$ concentrations on the assembly yield of the bundle[16] (Supporting Information Figure S4). 13 mM $MgCl_2$ was identified as optimum and corresponded to the typical concentration used for engineering DNA origami[50]. Next, we validated three different assembly procedures of the DNA origami: (i) a one-step assembly, leading to formation of a bundle equipped with both sets of ssDNA, hybridized to their corresponding bioreceptor and thiol-modified oligonucleotides, (ii) a two-step assembly, in which the bioreceptor and thiol-modified oligonucleotides were hybridized to the pre-assembled bundle bearing both ssDNA sets, for 1 h at 37 °C, and (iii) similar to the previous procedure but performing an intermediate PEG purification between the two assembly steps. The gel electrophoresis analysis indicates (Figure 2C), there were no clear differences between the stepwise assembly process (lanes 6 – 8 and 9 – 11) and the one-step assembly (lanes 3 – 5) neither for the LS nor for the DE origami, suggesting that both methods are equivalent. Aggregation along the helical axis was observed when the DE structure is formed with or without aptamer (traling bands in Figure C DE, line 2, 3, 6 and 9). This was also confirmed with AFM (data not included). By adding the thiolated ssDNA strand (single-step or afterwards in a second step) this aggregation along the helical axis disappeared. Although the one-step assembly method is easier and results in rapid assembly, we opted for the two-step method as it advantageous when preparing DNA origami structures for biosensing applications: origami structures

can be prepared without the thiol-modified ssDNA (dark red in figures), which are now first linked to the biosensor surface using common dithiothreitol (DTT)-based procedures with minimal damage for the DNA origami structures which are added afterwards using mild hybridization conditions (for more details, see Experimental section: FO-SPR).

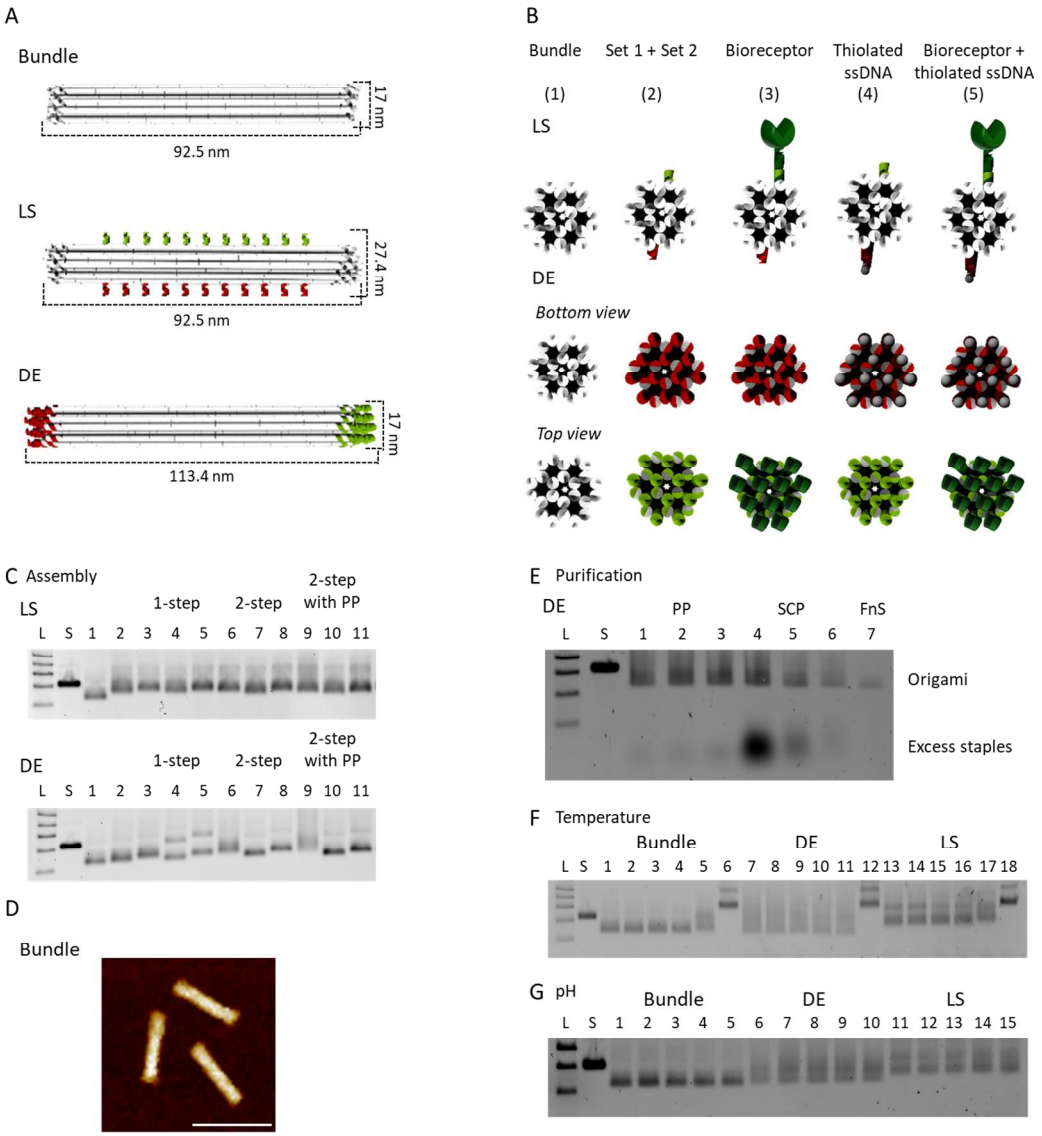

Figure 2: 3D DNA origami development and characterization. (A) Schematic representation of the 24-helix bundle, LS and DE DNA origami structures with strands of ssDNA set 1 (red) and set 2 (green). (B) Schematic illustrations of the LS and DE cross sections, representing the origami bundle (1), origami structure with addition of ssDNA set 1 and set 2 (2), origami with TBA bioreceptor (3), origami with thiol-modified ssDNA strands (4) and origami with TBA bioreceptor and thiol-modified ssDNA strands (5). (C) Characterization of 24-helix bundle, LS and DE structures using 1 % agarose gel. Labels: L, 1 kb DNA ladder; S, reference sample containing only scaffold strands; 1 – 5 numbers correspond to the origami structures presented in B; 3 – 5, 6 – 8 and 9 – 11 represent the same structures made following different methods: 1-step assembly process, 2-step assembly process or 2-step assembly with intermediate purification, respectively. (D) AFM image of the 24-helix bundle (scale bar: 100 nm). (E) Characterization of different purification methods for DE origami using 1 % agarose gel. Labels: L, 1 kb DNA ladder; S, reference sample containing only scaffold strands; 1 – 3, DE origami purified following PP method after incubating the pellet at 30 °C for 24, 12 and 0.5 h, respectively; 4 – 6, DE origami purified following SCP method with 1, 2 or 3 rounds of purification, respectively; 7, DE origami purified following FNS method. (F, G) Characterization of the stability of the 24-helix bundle, LS and DE origami in different buffer conditions using 1 % agarose gel. In both F and G: L, 1 kb DNA ladder; S, reference sample

containing only scaffold strands; F: 1 – 6 represent the 24-helix bundle conditioned in a temperature range from 20 until 70 °C (interval of 10 °C); 7 – 12 and 13 – 18 represent the same temperature experiment for DE and LS origami, respectively; G: 1 – 5 represent the 24-helix bundle conditioned in a pH range from 7 until 9 (interval of 0.5); 6 – 10 and 11 – 15 represent the same pH experiment for DE origami and LS origami, respectively.

In addition, the developed 24-helix bundle was analyzed using atomic force microscopy (AFM) (Figure 2D and Supporting Information Figure S5). The AFM images clearly show that the experimentally determined dimensions of the DNA origami structures (L: 99.5 ± 2.1 nm and W: 18.5 ± 1.7 nm, n = 190) well match the theoretical predictions (L: 92.5 nm, W: 17 nm). The overestimated lateral dimensions is most likely due to the finite radius of the AFM tip[51] combined with strong electrostatic attractions between the DNA origami and the mica surface under the non-native conditions used during AFM imaging.

Next, we purified the DNA origami structures to eliminate the excess of unbound staple strands and tested their stability at different pH and temperature values, as both aspects are important for correct incorporation of origami structures in bioassays. Because traditional gel extraction (Freeze 'N Squeeze DNA Gel Extraction Spin Columns, FNS) resulted in a suboptimal yield (Figure 2E, lane 7), different purification methods were examined, such as polyethylene glycol (PEG) purification (PP)[46] and spin column purification (SCP)[33]. Both of these methods allow, next to purification and concentration of the DNA origami solution, exchanging the solvent to buffer solutions typically used for biosensing. Following the protocols as detailed in the Experimental section, the PP approach resulted in the desired removal of the excess staple strands and a high recovery yield of the DNA origami after only one purification round (Figure 2E, lane 1-3), while the SCP required three rounds to obtain a similar purification grade with a much lower yield (Figure 2E, lane 4-6). Therefore, the PP method was selected for further purification of DNA origami structures. The presented results correspond to the DE origami structures, but the same high yield PP purification was also observed for the LS structures (data not shown). The stability of the DNA origami structures was further demonstrated by > 1 h incubation over a typical biosensing pH range (between 7 and 9) and a broad temperature range (between 20 and 70 °C) (Figure 2F and G). As shown in Figure 2F, denaturation of the different DNA origami structures started to occur only at temperature ≥ 60 °C (lanes 5 and 6; 11 and 12; 17 and 18 for the bundle, DE and LS, respectively). This is in agreement with previously published results showing that multilayered DNA origami structures have melting transitions between 50 and 65 °C, while reduced melting temperatures may be an indication of destabilizing factors or suboptimal design[32]. On the other hand, the range of pH values tested here did not have any impact on the stability of the DNA origami structures (Figure 2G).

In conclusion, we demonstrated here the successful synthesis and purification of different DNA origami structures with the required characteristics (modifications, stability, purity and yield) for biosensing applications.

3.2. Oriented attachment of targets to 3D DNA origami structures

To test whether 3D DNA origami can indeed be used for nanostructuring the biosensor surface with bioreceptors, we first examined whether we can control positioning of bioreceptors on the LS and DE origami structures. Hereto, we prepared three types of structures (Figure 3) starting from the basic LS and DE by binding gold nanoparticles (Au NPs), streptavidin or both to either of these origami structures. In this experiment, Au NPs were representing the gold biosensors surface (i.e. a surface for the attachment of the origami structures), whereas streptavidin was used to mark their opposite side (i.e. the side for immobilizing bioreceptors).

To do this, in a first step, we hybridized thiol-modified ssDNA oligonucleotides to the ssDNA set 1 (I and IV in Figure 3A representing LS and DE structures, respectively), biotinylated ssDNA oligonucleotides to the ssDNA set 2 (II and V corresponding to the LS and DE structures, respectively) or both types of oligonucleotides to ssDNA set 1 and 2 on the same structure (III and VI representing LS and DE structures, respectively). Stability of the obtained DNA origami structures was demonstrated by gel electrophoresis (Supporting Information Figure S6). In a second step, Au NPs, streptavidin or both were added to the LS and DE origami for topographical marking and characterization by AFM. As shown in the AFM images (Figure 3B and Supporting Information Figure S7), the designed LS and DE origami structures allowed attachment of Au NPs and streptavidin with nanoscale precision and predictable orientation.

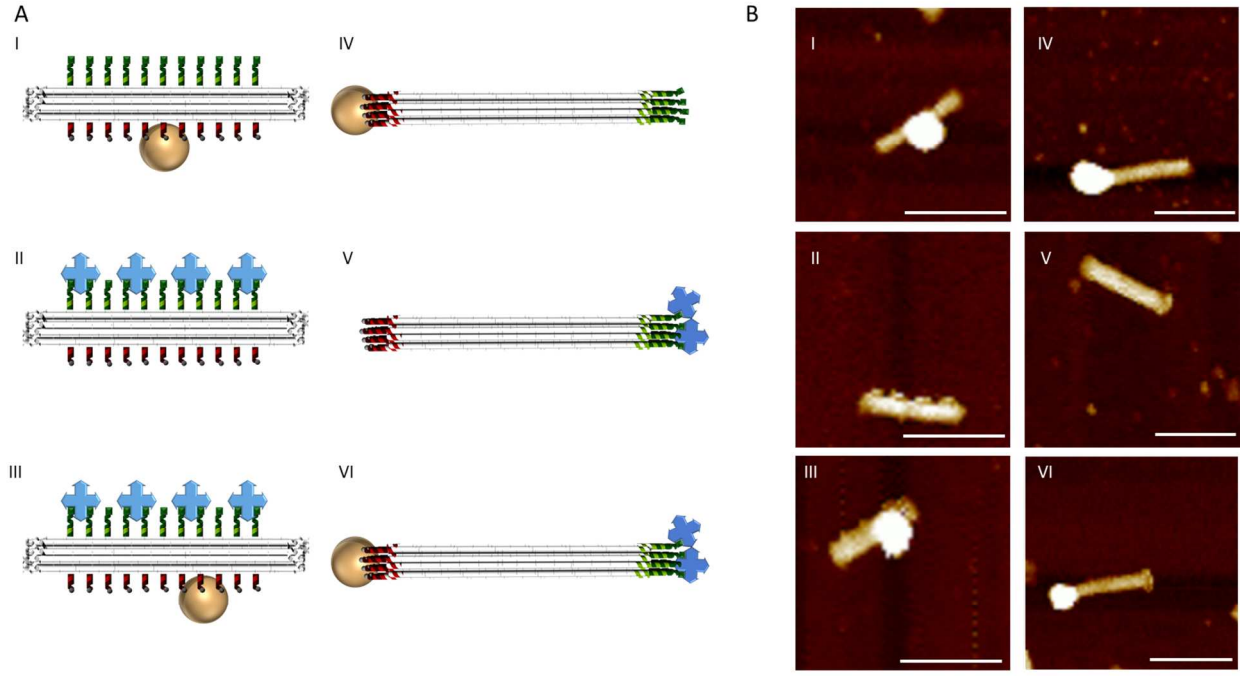

Figure 3*:* Controlled attachment of Au NPs and streptavidin to 3D DNA origami structures. (A) I, II and III, schematic representation of the LS origami structures hybridized to: thiol-modified ssDNA (dark red with grey spheres) for binding Au NPs (I), biotinylated ssDNA (dark green) for binding streptavidin (II) and both thiol-modified ssDNA and biotinylated ssDNA for simultaneous binding of Au NPs and streptavidin, respectively; IV, V and VI represent the same for the DE origami structures. (B) AFM images of structures I-VI, demonstrating highly controlled binding of Au NPs (I, IV), streptavidin (II, V) and both Au NPs and streptavidin (III, VI) to LS (I-III) and DE origami (IV-VI). Scale bars represent 100 nm.

3.3. FO-SPR bioassay development with DNA nanostructured biosensor

Next, we wanted to study the potential of 3D DNA origami for patterning a biosensor surface with bioreceptors in a highly controlled manner as well as the impact this might have on the performance of the biosensor. To do this, we functionalized the FO-SPR sensor tip with LS and DE origami structures, previously hybridized with the TBA bioreceptors. TBA was selected as a model system due to the high affinity towards its thrombin target (K_D = 0.5 nM)[45, 52]. As a reference, we functionalized the FO-SPR sensor tip with tetrahedron structures[47] containing TBA as pending probes (Figure 4A). This tetrahedron-mediated immobilization of bioreceptors was implemented for the first time on the FO-SPR biosensor and represented a preliminary step from traditional random functionalization of biosensor surfaces

towards highly ordered ones with predictable nanoscale precision through LS and DE origami structures (Figure 4A). Tetrahedrons were designed as described in Supporting information Figure S8 and S9.

Using such functionalized FO-SPR sensor tips, we first hybridized fluorescently labeled oligonucleotides to the TBA aptamer in order to visualize its presence and study its accessibility on these three types of DNA structures. It is important to note that FO-SPR sensor tips were prepared with and without PEG backfilling for all three structures. The microscopy images clearly show the presence of fluorescently labeled oligonucleotides in all tested conditions, demonstrating for the first time that indeed all three developed DNA structures could be successfully immobilized on the FO-SPR sensor tip (Figure 4B). Moreover, this also confirms that TBA aptamer immobilized on the FO-SPR sensor tip through DNA nanostructures is accessible for the hybridization with its complementary oligonucleotide.

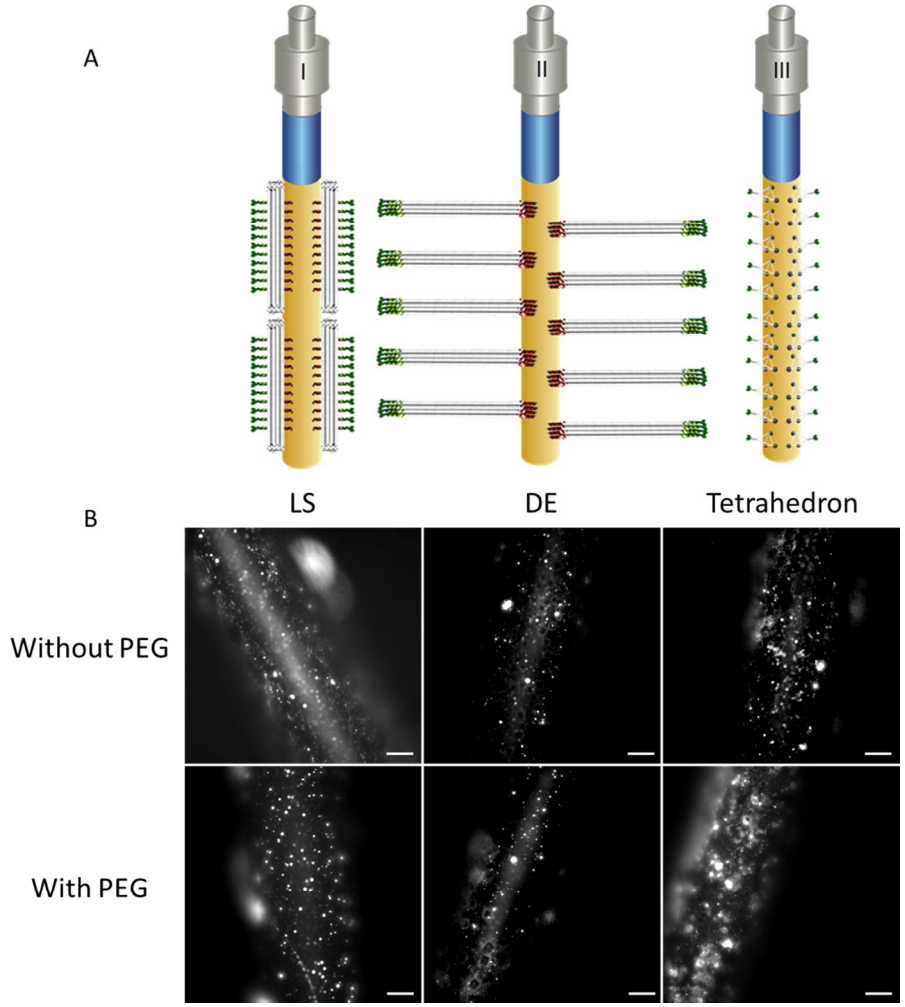

Figure 4: Functionalization of the FO-SPR biosensors with DNA nanostructures. (A) Conceptual overview of the FO-SPR biosensor configurations, namely TBA coupling through LS (I), DE (II) and tetrahedrons (III). (B) Fluorescence microscopy images of fluorescently labelled oligonucleotides hybridized to TBA-containing DNA structures coupled to FO-SPR sensor tips (with and without PEG backfilling). Scale bars represent 100 µm.

The performance of these six FO-SPR biosensor configurations was further validated in buffer by quantifying the range of thrombin concentrations (1 to 248 nM) that corresponds to the dynamic range of different thrombin bioassays described in literature[52]. The established calibration curves (with R^2

values ≥ 0.92 for all studied coupling methods) are depicted in Figure 5, whereas the obtained FO-SPR sensorgrams of all the bioassays are represented in Supporting Information Figure S10. One of the most remarkable observations from the calibration curves was that the FO-SPR sensor tips without PEG backfilling (black curves in Figure 5) performed significantly better for the high thrombin concentrations than those with PEG (red curves), irrespective of the DNA nanostructure immobilized on the sensor surface. Backfilling is commonly applied in biosensor development to decrease non-specific interactions, enhance upward orientation of bioreceptors and improve accessibility of the coupled bioreceptors. Moreover, it is known to reduce the available recognition sites on the sensor surface due to competition between the bioreceptors and PEG backfilling molecules for the available coupling groups at the biosensing surface, resulting in lower DNA densities and decreased signal-to-noise ratio (SNR)[53]. Contrary to the proven benefits of backfilling when immobilizing DNA bioreceptors directly on the biosensor surface, our results suggest that backfilling is not only unnecessary when nanostructuring the FO-SPR sensor tip surface with DNA tetrahedron and origami structures, but that it rather negatively affects the biosensors performance. This conclusion is further strengthened by calculating SNR that appears to be significantly lower (up to 50 %) for all three biosensor configurations with PEG compared to those without PEG (Table 1). These results are in agreement with previously published work of Pei et al.[12], showing that DNA tetrahedrons on flat gold surfaces for electrochemical detection increase the stability of surface-confined probes by approximately 5000 times without the need for backfilling (which was however needed for direct coupling of bioreceptors). It is important to note that the reproducibility of the FO-SPR biosensors performance was extremely high for all six tested conditions (Table 1), suggesting that the functionalization of the FO-SPR sensor tip surface with DNA nanostructures is a repeatable and greatly robust process.

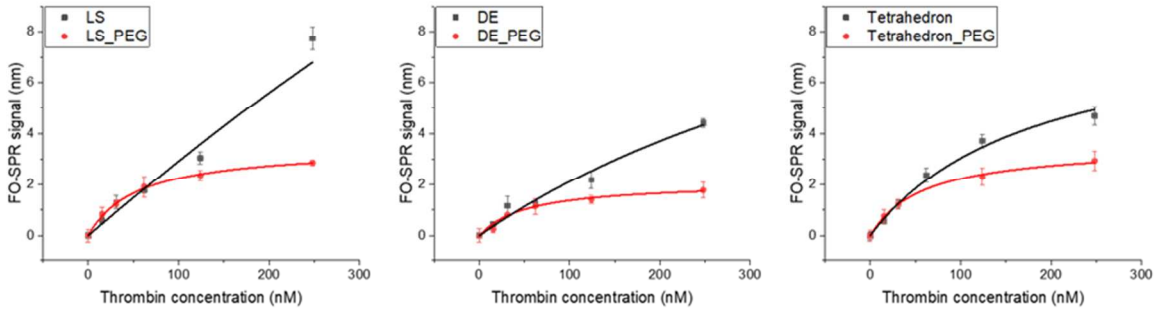

Figure 5: Thrombin bioassay on the FO-SPR biosensing platform. Calibration curves for thrombin established with the three different coupling methods of TBA to the FO-SPR biosensing surface without and with backfilling. Error bars in all graphs represent one standard deviation (n = 3).

When further comparing the performance of only the three FO-SPR biosensor configurations without PEG backfilling (as the better performing ones), it seems that a wider linear range is obtained for the DNA origami-based FO-SPR (especially the one with LS structures) compared to the tetrahedron-based biosensors. In other words, DNA origami-based sensors do not show saturation for the studied thrombin concentration range. This might be attributed to the controlled and/or higher density of the multiple bioreceptors per nanostructure and their upward orientation, resulting in lower steric hindrance and better bioreceptor accessibility. The obtained results therefore strongly suggest that DNA origami is a preferable method for bioreceptor immobilization on the biosensor surface.

Interestingly, the FO-SPR sensor tips with the LS DNA origami has the highest signal intensity among the three biosensors (when taken for the highest measured thrombin concentration, Table 1). Although TBA bioreceptors immobilized through tetrahedron structures lie closer to the sensor surface (8.5 nm) compared to the those introduced through LS origami (27 nm) or DE origami (113 nm), it seems that the LS DNA origami is more beneficial for specific and controlled attachment of bioreceptors. Moreover, the average occupied surface per aptamer on LS origami is 10 × larger compared to the average occupied space per aptamer on a tetrahedron. This is also in agreement with the widest linear range obtained with the same origami structures. However, further in depth studies are needed to reveal the best design and dimensions of DNA nanostructures for immobilizing bioreceptors on the FO-SPR surface, especially when taking into account well known correlation between signal intensity and distance of the biomolecular interaction from the SPR sensor surface[54]. Finally, the three FO-SPR biosensor configurations display a similar limit of detection (LOD), with DE exhibiting the lowest value due to the exceptionally small error obtained for the blank measurement (0 nM thrombin), which is taken into account for calculating LOD (see Equation 2 in Experimental section).

Table 1: Parameters of the thrombin bioassay using three different coupling methods. SNR represents the mean value calculated per calibration curve by taking the average of the SNR values for all concentrations. Reproducibility (nm) represents the mean standard deviation on the FO-SPR signal intensity per calibration curve, calculated by taking the average of the standard deviation from all the concentrations. Signal intensity (nm) is presented for the highest measured thrombin concentration of 248 nM. Coefficient of determination (R^2 value) was determined with Origin 8. LOD (nM) is calculated as specified in Experimental section, equation 2.

DNA nanostructure	**SNR**	**Reproducibility (nm)**	**Signal intensity (nm)**	**R^2**	**LOD (nM)**
Tetrahedron	9.8	0.22	4.68	0.99	10.7
Tetrahedron-PEG	6.1	0.27	2.94	0.99	13.8
LS	18.9	0.19	7.74	0.95	11.2
LS-PEG	11.4	0.23	2.85	0.99	15.0
DE	13.4	0.17	4.40	0.98	6.1
DE-PEG	6.9	0.21	1.78	0.92	30.7

In summary, we demonstrated the development of a functional thrombin FO-SPR biosensor by using DNA nanostructures, such as tetrahedrons and 3D DNA origami, as a new strategy to immobilize aptamer bioreceptors. Moreover, we showed that this functionalization approach does not rely on the backfilling process, previously recognized as an essential step towards obtaining functional biosensors. In addition, nanostructuring FO-SPR surfaces with DNA origami led to development of a biosensor with wider linear range compared to the ones with tetrahedrons, despite a lower amount of bioreceptors being positioned further away from the biosensing surface. Importantly, developed protocols for functionalization through these DNA nanostructures were highly reproducible and robust.

4. Conclusions

In this paper we have demonstrated an innovative strategy to couple bioreceptors to the biosensor surface with nanoscale precision using 3D DNA origami. Two different origami structures were first designed to achieve distinct distance of the bioreceptors from the biosensing surface, and effectively synthesized, purified and characterized through AFM. Both structures demonstrated stability over a range of temperatures and pH values next to the ability to control attachment of bioreceptors with nanoscale precision and predictable orientation. These well characterized structures were subsequently used to nanostructure the surface of a FO-SPR biosensor with a thrombin-specific aptamer. After

proving the presence of 3D DNA origami structures on the FO-SPR surface and the accessibility of the aptamer itself, the functionalized biosensors were evaluated for their performance when detecting range of thrombin concentrations. FO-SPR biosensors functionalized with tetrahedrons as carriers of the thrombin bioreceptors were used as a reference. All three types of developed biosensors revealed that backfilling is not necessary when immobilizing bioreceptors through DNA nanostructures and that the presence of PEG backfilling molecules even diminishes the biosensing performance. While functionalizing the FO-SPR surface proved to be very reproducible irrespective of the DNA nanostructures used, an increased detection range was obtained for the DNA origami compared to the tetrahedron-based biosensors. On the other hand, the calculated LOD was very similar for all developed biosensor configurations. In conclusion, our approach allows for the controlled engineering of rigid DNA origami to nanostructure biosensing interfaces and can be used to better understand the bioreceptor coupling process and to improve diagnostic sensing devices. Future work will focus on studying novel DNA origami structures resulting in the different bioreceptor densities, characterization of the packaging of the solid-state biosensor surface with DNA structures to improve biosensing and novel DNA origami-based biomolecular detection concepts.

Supporting Information

CaDNAno files showing the structural design details of the different origami structures; Schematic representation of the tetrahedron formation; Tables of the DNA sequences used in this work; Magnesium screening experiments; Validation of DNA origami core with AFM; Gel electrophoresis and AFM experiments to analyze oriented attachment of targets to DNA origami; Gel electrophoresis experiments to study DNA tetrahedron formation and FO-SPR sensorgrams of the developed thrombin bioassays.

Acknowledgements

We gratefully acknowledge financial support from KU Leuven (IOF/KP/12/002-Nanodiag; PDM/15/111 Devin Daems, OT 13/058), and Fund for Scientific Research (FWO G086114N, FWO-Flanders Postdoctoral Fellow Devin Daems 12U1618N, FWO-Flanders Research Stay Devin Daems V419416N, FWO-Flanders Doctoral grant Iene Rutten 1S30016N). We also thank financial support from the Deutsche Forschungsgemeinschaft (CRC 1093 initiative, project A6 and SA-1952/3-1 founded to B.S.)

Competing interests

The authors declare no competing financial interests

Corresponding authors

Correspondence to Jeroen Lammertyn (jeroen.lammertyn@kuleuven.be) and Dragana Spasic (dragana.spasic@kuleuven.be)

References

1. Turner, A. P. Biochemistry. Biosensors--sense and sensitivity. *Science* **2000**, *290*, 1315-1317.
2. Updike, S. J.; Hicks, G. P. The Enzyme Electrode. *Nature* **1967**, *214*, 986-988.
3. Clark, L. C.; Lyons, C. Electrode systems for continuous monitoring in cardiovascular surgery. *Annals of the New York Academy of Sciences* **1962**, *102*, 29–45.

4. John, A. S.; Price, C. P. Existing and Emerging Technologies for Point-of-Care testing. *Clin Biochem Rev* **2014**, *35*, 155-167.
5. Mascini, M.; Palchetti, I. *Nucleic Acid Biosensors for Environmental Pollution Monitoring*. Royal Society of Chemistry: Cambridge, U.K., 2011.
6. Chambers, J. P.; Arulanandam, B. P.; Matta, L. L.; Weis, A.; Valdes, J. J. Biosensor recognition elements. *Curr. Issues Mol. Biol.* **2008**, *10*, 1-12.
7. Seeman, N. C. Nucleic acid junctions and lattices. *J. Theor. Biol.* **1982**, *99*, 237-247.
8. Winfree, E.; Liu, F.; Wenzler, L. A.; Seeman, N. C. Design and self-assembly of two-dimensional DNA crystals. *Nature* **1998**, *394*, 539-544.
9. Chen, J. H.; Seeman, N. C. Synthesis from DNA of a molecule with the connectivity of a cube. *Nature* **1991**, *350*, 631-633.
10. Erben, C. M.; Goodman, R. P.; Turberfield, A. J. Single-molecule protein encapsulation in a rigid DNA cage. *Angew Chem Int Ed Engl* **2006**, *45*, 7414-7417.
11. Goodman, R. P.; Heilemann, M.; Doose, S.; Erben, C. M.; Kapanidis, A. N.; Turberfield, A. J. Reconfigurable, braced, three-dimensional DNA nanostructures. *Nat Nanotechnol* **2008**, *3*, 93-96.
12. Pei, H.; Zuo, X.; Pan, D.; Shi, J.; Huang, Q.; Fan, C. Scaffolded biosensors with designed DNA nanostructures. *NPS Asia Materials* **2013**, *5*, e51; doi:10.1038/am.2013.22.
13. Ge, Z.; Lin, M.; Wang, P.; Pei, H.; Yan, J.; Shi, J.; Huang, Q.; He, D.; Fan C.; Zuo, X. Hybridization chain reaction amplification of microRNA detection with a tetrahedral DNA nanostructure-based electrochemical biosensor. *Anal. Chem.* **2014**, *86*, 2124-2130.
14. Lin, M.; Wang, J.; Zhou, G.; Wang, J.; Wu, N.; Lu, J.; Gao, J.; Chen, X.; Shi, J.; Zuo, X.; Fan, C. Programmable Engineering of a Biosensing Interface with Tetrahedral DNA Nanostructures for Ultrasensitive DNA Detection. *Angew. Chem. Int. Ed.* **2015**, *54*, 2151-2155.
15. Rothemund, P. W. Folding DNA to create nanoscale shapes and patterns. *Nature* **2006**, *440*, 297-302.
16. Douglas, S. M.; Dietz, H.; Liedl, T.; Hogberg, B.; Graf, F.; Shih, W. M. Self-assembly of DNA into nanoscale three-dimensional shapes. *Nature* **2009**, *459*, 414-418.
17. Shih, W. M.; Lin, C. Knitting complex weaves with DNA origami. *Curr Opin Struct Biol* **2010**, *20*, 276-282.
18. Torring, T.; Voigt, N. V.; Nangreave, J.; Yan, H.; Gothelf, K. V. DNA origami: a quantum leap for self-assembly of complex structures. *Chem Soc Rev* **2011**, *40*, 5636-5646.
19. Sacca, B.; Niemeyer, C. M. DNA origami: the art of folding DNA. *Angew Chem Int Ed Engl* **2012**, *51*, 58-66.
20. Kuzyk, A;, Schreiber, R.; Fan, Z.; Pardatscher, G.; Roller, E.-M.; Högele, A.; Simmel, F. C.; Govorov, A. O.; Liedl, T. DNA-based self-assembly of chiral plasmonic nanostructures with tailored optical response. *Nature* **2012**, *483*, 311-314.
21. Schiffels, D.; Liedl, T.; Fygenson, D. K. Nanoscale structure and microscale stiffness of DNA nanotubes. *ACS Nano* **2013**, *7*, 6700-6710.
22. Schreiber, R.; Santiago, I.; Ardavan, A.; Turberfield, A. J. Ordering gold nanoparticles with DNA origami nanoflowers. *ACS NANO* **2016**, *10*, 7303-7306.
23. Zhan, P.; Dutta, P. K.; Wang, P.; Song, G.; Dai, M.; Zhao, S-X.; Wang, Z-G.; Yin, P.; Zhang, W.; Ding, B.; Ke, Y. Reconfigurable Three-Dimensional gold nanorod plasmonic nanostructures organized on DNA origami tripod. *ACS NANO* **2017**, *11*, 1172-1179.
24. Lin, C.; Katilius, E.; Liu, Y.; Zhang, J.; Yan, H. Self-assembled signaling aptamer DNA arrays for protein detection. *Angew Chem Int Ed Engl* **2006**, *45*, 5296-5301.
25. Lin, C.; Liu, Y.; Yan, H. Self-assembled combinatorial encoding nanoarrays for multiplexed biosensing. *Nano Lett* **2007**, *7*, 507-512.

26. Godonoga, M.; Lin, T-Y.; Oshima, A.; Sumitomo, K.; Tang, M. S. L.; Cheung, T-W.; Kinghorn, A. B.; Dirkzwager, R. M.; Zhou, C.; Kuzuya, A.; Tanner, J. A.; Heddle, J. G. A DNA aptamer recognising a malaria protein biomarker can function as a part of a DNA origami assembly. *Sci. Rep.* **2016**, *6*, 21266.
27. Rothemund, P. W.; Papadakis, N.; Winfree, E. Algorithmic self-assembly of DNA Sierpinski triangles. *PLoS Biol* **2004**, *2*, e424.
28. Schuller, V. J.; Heidegger, S.; Sandholzer, N.; Nickels, P. C.; Suhartha, N. A.; Endres, S.; Bourquin, C.; Liedl, T. Cellular immunostimulation by CpG-sequence-coated DNA origami structures. *ACS Nano* **2011**, *5*, 9696-9702.
29. Sellner, S.; Kocabey, S.; Nekolla, K.; Krombach, F.; Liedl, T.; Rehberg, M. DNA nanotubes as intracellular delivery vehicles in vivo. *Biomaterials* **2015**, *53*, 453-463.
30. Douglas, S. M.; Bachelet, I.; Church, G. M. A logic-gated nanorobot for targeted transport of molecular payloads. *Science* **2012**, *335*, 831-834.
31. Modi, S.; Swetha, M. G.; Goswami, D.; Gupta, G. D.; Mayor, S.; Krishnan, Y., A DNA nanomachine that maps spatial and temporal pH changes inside living cells. *Nat Nanotechnol* **2009**, *4*, 325-330.
32. Castro, A. E.; Kilchherr, F.; Kim, D-N.; Shiao, E. L.; Wauer, T.; Wortmann, P.; Bathe, M.; Dietz, H. A primer to scaffolded DNA origami. *Nature Methods* **2011**, *8*, 221-229.
33. Fu, Y.; Zeng, D.; Chao, J.; Jin, Y.; Zhang, Z.; Liu, H.; Li, D.; Ma, H.; Huang, Q.; Gothelf, K. V.; Fan, C. Single-step rapid assembly of DNA origami nanostructures for addressable nanoscale bioreactors. *J. Am. Chem. Soc.* **2013**, *135*, 696-702.
34. Puchkova, A.; Vietz, C.; Pibiri, E.; Wünsch, B.; Sanz Paz, M.; Acuna, G. P.; Tinnefeld, P. DNA Origami Nanoantennas with over 5000-fild Fluorescence enhancement and single-molecule detection at 25 µM. *Nano Lett.* **2015**, *15*, 8354-8359.
35. Ochmann, S. E.; Vietz, C.; Trofymchuk, K.; Acuna, G. P.; Lalkens, B.; Tinnefeld, P. Optical nanoantenna for single molecule-based detection of zika virus nucleic acids without molecular multiplication. *Anal. Chem.* **2017**, *89*, 13000-13007.
36. Torelli, E.; Manzano, M.; Srivastava, S. K.; Marks, R. S. DNA origami nanorobot fiber optic genosensor to TMV. *Biosens & Bioelectron* **2017**, *99*, 209-215.
37. Pollet, J.; Janssen, K. P. F.; Knez, K.; Lammertyn, J. Real-time monitoring of solid-phase PCR using fiber-optic SPR. *Small* **2011**, *7*, 1003-1006.
38. Lu, J.; Van Stappen, T.; Spasic, D.; Delport, F.; Vermeire, S.; Gils, A.; Lammertyn, J. Fiber optic-SPR platform for fast and sensitive infliximab detection in serum of inflammatory bowel disease patients. *Biosens Bioelectron* **2016**, *79*, 173-179.
39. Pollet, J.; Delport, F.; Janssen, K. P. F.; Tran, D.T.; Wouters, J.; Verbiest, T.; Lammertyn, J. Fast and accurate peanut allergen detection with nanobead enhanced optical fiber SPR biosensor. *Talanta* **2011**, *83*, 1436–1441.
40. Tran, D. T.; Knez, K.; Janssen, K. P. F.; Pollet, J.; Spasic, D.; Lammertyn, L. Selection of aptamers against Ara h 1 protein for FO-SPR biosensing of peanut allergens in food matrices. *Biosens Bioelectron* **2013**, *43*, 245–251.
41. Knez, K.; Janssen, K. P. F.; Pollet, J.; Spasic, D.; Lammertyn, J. Fiber-optic high-resolution genetic screening using gold-labeled gene probes. *Small* **2012**, *8*, 868-872.
42. Knez, K.; Janssen, K. P. F.; Spasic, D.; Declerck, P.; Vanysacker, L.; Denis, C.; Tran, D. T.; Lammertyn, J. Spherical nucleic acid enhanced FO-SPR DNA melting for detection of mutations in Legionella pneumophila. *Anal Chem* **2013**, *85*, 1734-1742.
43. Daems, D.; Knez, K.; Delport, F.; Spasic, D.; Lammertyn, J. Real-time PCR melting analysis with fiber optic SPR enables multiplex DNA identification of bacteria. *Analyst* **2016**, *141*, 1906-1911.
44. Douglas, S. M.; Marblestone, A. H.; Teerapittayanon, S.; Vazquez, A.; Church, G. M.; Shih, W. M. Rapid prototyping of 3D DNA-origami shapes with caDNAno. *NAR* **2009**, *37*, 5001-5006.

45. Pfeifer, W.; Lill, P.; Gatsogiannis, C.; Saccà, B. Hierarchical assembly of DNA filaments with designer elastic properties. *ACS Nano* **2018**, *12*, 44-55.
46. Stahl, E.; Martin, T. G.; Praetorius, F.; Dietz, H. Facile and scalable preparation of pure and dense DNA origami solutions. *Angew. Chem. Int. Ed.* **2014**, *53*, 12735-12740.
47. Pei, H.; Lu, N.; Wen, Y.; Song, S.; Liu, Y.; Yan, H.; Fan, C. A DNA Nanostructure-based biomolecular probe carrier platform for electrochemical biosensing. *Advanced Materials* **2010**, *9*, 4754-4758.
48. Tasset, D. M.; Kubik, M. F.; Steiner, W. Oligonucleotide inhibitors of human thrombin that bind distinct epitopes. *J. Mol. Biol.* **1997**, *272*, 688-698.
49. Pfeifer, W.; Saccà, B. From Nano to Macro through Hierarchical self-assembly: the DNA Paradigm. *ChemBioChem* **2016**, *12*, 1063-1080.
50. Martin, T. G.; Dietz, H. Magnesium-free Self-assembly of Multilayer DNA objects. *Nat. Commun.* **2012**, *3*, 1103.
51. Severin, N.; Dorn, M.; Kalachev, A.; Rabe, J.P. Replication of single macromolecules with graphene. *Nano Lett* **2011**, *11*, 2436-2439.
52. Deng, B.; Lin, Y.; Wang, C.; Li, F.; Wang, Z.; Zhang, H.; Li, W-F.; Chris Le, X. Aptamer binding assays for proteins: The thrombin example – A review. *Anal. Chim. Acta* **2014**, *837*, 1-15.
53. Janssen, K. P. F.; Knez, K.; Vanysacker, L.; Schrooten, J.; Spasic, D.; Lammertyn, J. Enabling fiber optic serotyping of pathogenic bacteria through improved anti-fouling functional surfaces. *Nanotechnology* **2012**, *23*, 265503-2355109.
54. Homola, J. Surface Plasmon Resonance sensors for detection of chemical and biological species. *Chem. Rev.* **2008**, *108*, 462-493.

Graphic for manuscript